Investigational
Medicinal Chemistry & Pharmacology

Research Article Open Access

In-silico study of aminobenzoic acid Schiff base copper-complexes as potential cell inhibitors of cyclin-dependent kinase 7

Felicia Ndidi Ejiah[1]*, Oluwafemi Segun Aina[2], Inemesit Asukwo Udofia[3], Tolulope Mojisola Fasina[1], Oluwole Babafemi Familoni[1]

Abstract

Background: Cell inhibitors are gradually becoming a tool in drug discovery as this gives a lead to potential compounds with therapeutic application. Presently, cancer cell inhibitors have shown drug-likeness based on oral bioavailability, pharmacokinetics, global chemical reactivity and theoretical binding affinities. Herein, we report copper complexes synthesized from aminobenzoic acid moiety, *3-(2-hydroxybenzylideneamino) benzoic acid copper complex and 4-(2-hydroxybenzylideneamino) benzoic acid copper complex* as potential cell inhibitors of cyclin-dependent kinase 7.

Methods: The complexes were synthesized by condensation of 2-hydroxybenzylideneamino benzoic acid moiety Schiff bases with copper(II) chloride and characterized using Fourier Transform Infrared Spectroscopy, Electrospray ionization mass spectrometry, and ultraviolet-vis spectroscopy. The complexes were optimized using the M062X functional and GENECP basis set. DNA study was carried out on calf thymus DNA using circular dichroism. Human cyclin-dependent kinase 7 was processed using BIOVIA Discovery Studio 2020, docking simulations were conducted utilizing PyrxAutoDock. Independent runs at complex binding sites were assessed and ranked utilizing the Vina scoring function.

Results: The planar geometry of the complexes was validated by Density Functional Theory calculations. Results of analysis showed that both copper complexes are less toxic and exhibited higher binding energies to amino acid residues of cyclin-dependent kinase 7 when compared with all reference drugs, Epirubicin, Capecitabine, and 5-Fluorouracil. DNA study revealed minor groove binding to copper complexes via hydrogen bonding and validated by molecular docking.

Conclusion: 3-(2-hydroxybenzylideneamino) benzoic acid copper complex and 4-(2-hydroxybenzylideneamino) benzoic acid copper complex has shown potential activities that can inhibit cyclin-dependent kinase 7 in cancer therapy.

Keywords: Cancer; DFT calculations; DNA binding; molecular docking; synthesis.

*Correspondence: Tel.: +2349060002998; E-mail address: fejiah@unilag.edu.ng; ORCID: https://orcid.org/0000-0001-7727-522X (Felicia Ndidi Ejiah)
[1]Chemistry Department, University of Lagos, Akoka, Lagos, Nigeria; [2]Dept of Biological Science, Trinity University, Lagos, Nigeria; [3]Department of Chemistry and Biochemistry, Caleb University, Imota, Ikorodu LGA, Lagos State, Nigeria

Other authors
Email: oluwafemi.aina@trinityuniversity.edu.ng; ORCID: https://orcid.org/0000-0002-2988-6496 (Oluwafemi Segun Aina); Email: inemesit4god@gmail.com; ORCID: https://orcid.org/0000-0001-8304-1964 (Inemesit Asukwo Udofia); Email: tfasina@unilag.edu.ng; ORCID: https://orcid.org/0000-0001-7615-9083 (Tolulope Mojisola Fasina); Email: familonio@unilag.edu.ng; ORCID: https://orcid.org/0000-0002-5480-232X (Oluwole Babafemi Familoni).

Citation on this article: Ejiah FN, Aina OS, Udofia IA, Fasina TM, Familoni OB. In-silico study of aminobenzoic acid Schiff base copper-complexes as potential cell inhibitors of cyclin-dependent kinase 7. Investigational Medicinal Chemistry and Pharmacology (2025) 8(1):106; Doi: https://dx.doi.org/10.31183/imcp.2025.00106

Background

The development of new complexes with potential as inhibitors of human cyclin-dependent kinase 7 (CDK 7) prompted a great interest in this research, considering the biological importance of this protein in cancer therapy. Human cyclin-dependent kinase 7 is a member of the cyclin-dependent protein kinase family which regulates the activities of other CDKs through phosphorylation on their activation segment and hence contributes to control of the eukaryotic cell cycle. It is often overexpressed in various cancers, making it a promising target for cancer treatment due to its involvement in both transcription and cell cycle regulation [1]. Human cyclin-dependent kinase is an essential component of the transcription factor involved in transcription initiation and DNA repair. For maximum activity and stability, CDK7 requires phosphorylation in association with cyclin H. It also plays a central role in the regulation of the initiation phase of messenger RNA synthesis by RNA pol II [2] phosphorylating RNA polymerase II (RNA pol II) large subunit C-terminal domain (CTD) [3, 4]. Recently, the design and highly specific inhibitors of CDK7 have been instrumental in revealing the potential of CDK7 as a cancer drug target [5]. Cell cycle and transcription which are required for cancer progression can be regulated via cyclin-dependent kinase 7 as these have been evaluated in clinical trials [6]. Preclinical studies have revealed that cancer cells can be targeted by transcriptional inhibition because they are more reliant than normal cells and as such regulate cancer cell proliferation and survival [7, 8]. Presently, four CDK7 inhibitors, namely ICEC0942 [9] SY-1365 [10] SY-5609 [11] and LY340515 [5] have progressed to Phase I/II clinical trials for the treatment of advanced malignancies. Several functions of CDK7 [5] include regulating of cell cycle by phosphorylation [12, 9, 13] gene expression [14] and expression in tumors [14]. Previously, some Pan-CDK inhibitors such as flavopiridol [15, 16] and aminothiazole based compound [17] have been reported though pre-clinical studies have suggested improved efficacy with longer drug exposure as only marginal activity was demonstrated. It was also opinioned that Pharmacokinetic factors, such as binding of the drug to plasma proteins, may have limited its activity [15]. One of the main factors hindering the further clinical development of early-generation CDKIs was their lack of selectivity, which results in increased toxicity [17].

Development of new CDK7 inhibitory compounds has become necessary to facilitate the pharmaceutical development of new cancer drugs and minimize undesirable adverse effects to treat cancers which have acquired resistance to other drugs. A search through literature shows that Schiff bases and their metal complexes have not received much attention as CDK7 cell inhibitors in cancer therapy, despite the low toxicity reported for most Schiff base metal complexes [18, 19]. Schiff bases are compounds containing the imine functional group. Over the years, several biological activities have been reported [19], also the mechanism of action have reported DNA binding and cleavage [20] especially in the development of cancer drugs [21, 22].

The aim of this work is to synthesize and investigate in-silico Schiff base copper complexes of aminobenzoic acid moiety as CDK 7 inhibitors in cancer therapy. This would add to the literature and lay foundation for further research into this class of compounds for in-vitro study.

Methods

Materials

The chemicals and reagents used were purchased from Sigma-Aldrich chemical Co Ltd and used without further purification. They include ethanol, copper (II) chloride dihydrate $CuCl_2.2H_2O$. Electrospray Ionisation (ESI) analyses were performed in positive ionisation mode on a Micromass LCT Time of Flight Mass Spectrometer; Fourier Transform Infrared spectroscopy (FTIR) of the compounds were recorded on the spectrometer in the range of 4000 to 400 cm^{-1} using Perkin Elmer FTIR Spectrum Version10.4.00. All the characterizations were carried out at the University of Birmingham, United Kingdom.

3-(2-hydroxybenzylideneamino) benzoic acid (**S1)**, 4-(2-hydroxybenzylideneamino) benzoic acid **(S2)** were previously synthesized, characterized and used as starting material in this work.

Synthesis of Schiff bases

Schiff bases synthesized from salicylaldehyde and 3-aminobenzoic acid (**S1**), salicylaldehyde and 4-aminobenzoic acid (**S2**) have been reported by Ejiah et al [23].

Synthesis of Schiff base copper complexes

An ethanolic (40 ml) solution of Schiff base (4 mmol.) was mixed with Cu(II) chloride (2 mmol.) in ethanol (20 ml) solution keeping ligand-metal ratio 2:1. The solution was made alkaline with triethlyamine and heated to reflux for 4 h. The solid product formed was collected by filtration, washed in ethanol, dried and stored in a desiccator over silica gel. This afforded the desired product.

3-(2-hydroxybenzylideneamino) benzoic acid copper complex (S1-Cu)

Yield: 83 %; CHN Analyses: calculated: $C_{28}H_{20}CuN_2O_6$: C, 61.82; H, 3.71; N, 5.15. Found: C, 61.36; H, 3.52; N, 5.48; 5.25; ESI-MS: 544.06; m/z: 543.06 (100.0%), 545.06 (44.8%), 544.07 (30.7%), 546.06 (13.9%), FTIR (cm^{-1}); 3065, 1686, 1611, 1554, 1285, 1188, 904, 753, 693, 545, 485; UV-vis_{nm} (DMSO): 352 ($n\rightarrow\pi^*$), 406 ($d\rightarrow d$)

4-(2-hydroxybenzylideneamino) benzoic acid copper complex (S2-Cu)

Yield: 77 %; CHN Analyses: calculated: $C_{28}H_{20}CuN_2O_6$: C, 61.82; H, 3.71; N, 5.15. Found: C, 61.36; H, 3.52; N, 5.48; 5.25; ESI-MS: 544.06; m/z: 543.06 (100.0%), 545.06 (44.8%), 544.07 (30.7%), 546.06 (13.9%), FTIR (cm^{-1}); 3059,1598, 1533, 1390, 1153, 754, 574, 472; UV-vis_{nm} (DMSO): 324 ($n\rightarrow\pi^*$), 412 ($d\rightarrow d$)

Biophysical Experiment

Ultrapure water was used throughout all biophysical work. DNA samples were made up from Calf thymus DNA sodium salt (sigma Aldrich) by dissolving in milli-Q water and washed using a 10kda MWCO centrifuge tube. The solution was then quantified by UV-vis spectroscopy (Cary 5000 NIR spectrometer) by ε258 = 13200 mol^{-1} dm^3 cm^{-1} to give a concentration in DNA base pairs. This stock solution was kept in the fridge with fresh aliquot being taken out for each experiment. Fresh buffer was made up before each

experiment. Cobalt complexes were dissolved in 1% DMSO with fresh solutions being used for each batch of experiments.
Circular dichroism (CD) spectra were recorded on a Chirascan+ spectrometer (Applied Photophysics limited). The samples were scanned in a 1 cm path length cuvette between 400 and 200 nm with 3 repeats at 1 nm step size and 0.5 s dwell time S37 per point. Titrations were carried out at a constant concentration of DNA, sodium chloride (40 mM) and Tris HCl buffer (200 mM, pH 7.4) by adding compensating solutions of 2x DNA/Buffer of equal volume to the titre of the complex solution. The concentration of complex in the cuvette was increased step wise by adding set volumes of a stock complex solution. The R value refers to the ratio of DNA base pairs to complex, i.e. R60 = 60bp for every 1 complex, R4 = 4bp per complex

DFT Calculations-Geometry Optimization

The geometries of **S1-Cu** and **S2-Cu** were optimized in their ground states using the M062X functional [24] and the GENECP basis set. For Cu atom, the LANL2MB basis set was employed, while 6-31G* [25] was used for C, O, H, and N atoms. To verify the accuracy of these geometries, vibrational frequency calculations using second-order analytical derivatives was employed. A tight convergence criterion was enforced during the self-consistent field (SCF) calculations. To determine the absorption spectral properties of these compounds, the time-dependent density functional theory (TD-DFT) calculations were carried out on the optimized geometries at the M062X/GENECP level in acetonitrile. Solvation effects were modelled using the Integral Equation Formalism Polarizable Continuum Model (IEFPCM) for solvation. All theoretical simulations were carried out using the Gaussian 16 software package, with computational resources provided by SEAGrid [26, 27, 28].

Molecular Reactivity Descriptors

Single-point energy calculations were performed on the neutral, cationic, and anionic forms of the molecules at the M062X/GENECP level to determine their electronic energies. Following this, the polarizability (α), global molecular electrophilicity index (ω), global hardness (η), chemical potential (μ), vertical ionization potential (VIP), and vertical electron affinity (VEA) were calculated for **S1-Cu** and **S2-Cu**. A tight convergence criterion was applied for the SCF calculations, and the molecular descriptors were obtained using Equations 1-5, in the gas phase.

$$\text{Vertical Ionization Potential (VIP)} = E(N-1) - E(N) \quad (1)$$

$$\text{Vertical Electron Affinity (VEA)} = E(N) - E(N+1) \quad (2)$$

where, E(N – 1), E(N) and E(N+1) are the energies corresponding to (N – 1), (N) and (N+1) electron systems respectively.

$$\eta = \text{VIP} - \text{VEA} \quad (3)$$

$$\mu = -\frac{(\text{VIP}+\text{VEA})}{2} \quad (4)$$

$$\omega = \frac{(\mu)^2}{2\eta} \quad (5)$$

Docking Methodology

Selection of cancer protein receptor

The crystal structure of the human cyclin-dependent kinase 7 (CDK7) (an essential component of the transcription factor involved in transcription initiation and DNA repair) (PDB ID: 1UA2) HAP protein molecule, with a resolution of 3.02 Å was acquired from the Protein Data Bank at rcsb.org [13, 14]. The structure was obtained in the pdb format and subsequently processed using BIOVIA Discovery Studio DS 2020 to eliminate any unwanted ligands and water molecules. In addition, polar hydrogen atoms were added to the structure as required.

Preparation of complexes and docking

Docking simulations were conducted utilizing PyrxAutoDock, employing the Lamarkian genetic algorithm and default protocols for docking a flexible complex to a rigid protein. Initially, blind docking was performed to pinpoint potential binding sites on the target protein within a 75 × 75 × 75 cubic grid centered on the protein, encompassing its entirety. A grid spacing of 1.00 Å was utilized to calculate the grid maps via the autogrid module of AutoDock tools. For each complex and reference drug, energy minimization and conversion into protein data bank partial charge and atom type (pdbqt) format were executed. Subsequently, nine (9) independent runs of the protein were carried out against all complexes and reference drugs, whose structures were drafted using Chemdraw 14.0 and saved in simulation description format (SDF). Based on the identified potential binding sites, energetically favorable binding conformations were chosen using AutodockVina [29]. Docking of complexes to these sites commenced after potential binding sites were recognized, aiming to determine the most probable and energetically favorable binding conformations [30]. Independent runs at complex binding sites were assessed and ranked utilizing the Vina scoring function. The binding modes, accompanied by their respective binding affinities and RSB (upper and lower) values, were acquired to facilitate the selection of the highest scoring binding conformation for each complex. The binding mode with the optimum binding affinity was selected. All software applications were executed on PC-based machines operating the Microsoft Windows 10 operating system. Resulting structures were visualized and analyzed using DS visualizer.

Results and Discussion

Synthesis and characterization of Schiff base copper complexes

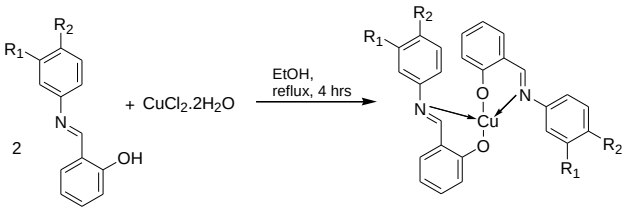

R_1=COOH, R_2=H, S1-Cu
R_1=H, R_2=COOH, S2-Cu

Scheme 1. Synthesis of Schiff base copper complexes

The Schiff base copper complexes were synthesized by refluxing each Schiff base ligand with copper(II) metal salt as shown in Scheme 1. Both complexes are represented in Figure 1.

ESI-MS

ESI-MS confirmed the exact mass and structures of the compounds as the found and calculated were in good agreement. Evident from Figures 2 and 3 are ESI-MS of **S1-Cu**, 544.0677, 545.0648 544.0748 and **S2-Cu**, 544.0677, 545.0648, 544.0646 respectively. Their m/z $[M+H]^+$544.06 (100.0%); 545.06 (44.8%), 544.07 (30.7%), 546.06 (13.9%) for **S1-Cu** and $[M+H]^+$ 544.06 (100.0%); 545.06 (44.8%), 544.07 (30.7%), 546.06 (13.9%) for **S2-Cu** complex.

FTIR

The IR spectra of the Schiff bases and copper complexes are presented in Figures 4. The Schiff base ligands, S1 and S2 displayed bands at 3059-3065 cm^{-1}, 1685 cm^{-1}, 1604-1613 cm^{-1} and 1184-1179 cm^{-1} which is characteristic of the OH, $C=O_{acid}$, C=N, -C-OH group respectively. Absence of the band at 1720-1740 cm^{-1} due to $C=O_{aldehyde}$ indicates the formation of the Schiff bases. On coordination to copper(II) metal ion, a shift in imine band was observed in the range 1611-1598 cm^{-1}, and 1188-1153 cm^{-1} suggesting that the copper ion coordinated via the imine nitrogen and hydroxyl oxygen. Bands associated to Cu-O and Cu-N bonds was observed around 545-574 cm^{-1} and 472-485 cm^{-1} respectively.

UV-spectroscopy

The UV-visible measurement was carried out between 200-600 nm at room temperature using DMSO as solvent. The UV-vis spectrum of **S1** and **S1-Cu** are shown in Figure 5A. The solution of the free ligands **S1** gave peak at 271 and 343 nm, which is attributed to π→ π* and n → π* transitions of the aromatic ring and non-bonding electrons present on the nitrogen of imine functional group respectively [31]. On coordination with copper(II) metal ion, a shift to lower energy band was observed for imine nitrogen (352 nm) and a new band around 406 nm confirming the coordination of the metal ion to the ligand. A similar trend was observed for **S2** and **S2-Cu** (Figure 5B). Coordination of metal ion to ligands can lead to shift in bands either to lower or higher energy, in addition to appearance of new bands due to *d→d* transitions. Also, weak and broad absorption bands in the lower energy (400-500 nm) can be ascribed to the spin-allowed metal-to-ligand charge transfer (MLCT), supporting coordination [32].

S2 free ligand exhibited two absorption bands, 281 and 351 nm attributed to π→ π* and n → π*, which on coordination to copper(II) metal ion, the imine band shifted to 324 nm with a new band around 412 nm due to *d→d* confirming complex formation.

Optimized structure

The optimized structures of compounds **S1-Cu** and **S2-Cu** are presented in Figure 6. The influence of substitution on the copper complex is evident in the bond angles and lengths near the central metal and nitrogen atom connected to the substituted ring. In structure (a), the C-N bond angles are computed to be 120.69˚ and 120.24˚, which are larger than the corresponding angles in structure (b), recorded at 118.63˚ and 118.28˚ respectively. This difference is expected because the –COOH substitution in (a) is positioned meta to the imine group, whereas in (b), it is positioned para to the imine group. The variation arises from a stronger electronic effect due to resonance, which is more pronounced at the para position than at the meta position, where such resonance is absent. In addition, this resonance effect contributes to the planar geometry of (b), resulting from a more extensive electron distribution along the imine compared to (a). A similar interplay of electronic and resonance effects accounts for the slightly longer C-N imine bond lengths in (b) compared to (a).

Global Molecular Descriptors and Electronic Properties

Table 1 presents the global molecular properties and frontier molecular orbital energies of **S1-Cu** and **S2-Cu**. These include the electronic energies of the neutral molecule (with N electrons), the cation (N-1 electrons, after losing one electron), and the anion (N+1 electrons, after gaining one electron). The more negative electronic energy, E(N), of **S1-Cu** suggests slightly greater thermodynamic stability compared to **S2-Cu**, with an energy difference of 0.0035 atomic units (equivalent to 9.2 kJ/mol). This small difference arises from substitution effects: the meta-substituted **S1-Cu** benefits from stabilization via an inductive effect, whereas the para-substituted **S2-Cu** does not exhibit the same degree of stabilization. Despite their similar thermodynamic stability, reflected in the small E(N) difference, **S2-Cu's** larger energy gap indicates greater kinetic stability, a critical factor for applications in materials science or biology.

S1-Cu exhibits a higher VIP value, indicating that it is more resistant to oxidation, and a higher VEA, suggesting a greater tendency to accept an electron. These trends align with observations in copper Schiff base complexes, as noted by Richter *et al*. [33]. η, which measures resistance to charge transfer, is higher in **S2-Cu**, reflecting greater stability and lower reactivity, consistent with its larger E_{gap}. In contrast, the more negative μ value of **S1-Cu** indicates it is a less effective electron donor, in line with its higher VIP. Additionally, the higher ω value **S1-Cu** points to stronger electrophilic behaviour, which could be advantageous in catalytic applications. The large E_{gap} observed in **S2-Cu** suggests greater kinetic stability and lower reactivity, a pattern frequently observed in metal complexes [34]. The energy gap, ranging from 5.5 to 5.8 eV, implies absorption in the ultraviolet region, a characteristic feature of Schiff base complexes. In **S2-Cu**, para-substitution enhances resonance with the salicylaldehyde moiety, elevating the LUMO energy and thereby increasing both E_{gap} and η. Conversely, the meta-substitution in **S1-Cu**, which lacks direct conjugation, exerts a stronger inductive effect, leading to a higher dipole moment and electrophilicity.

The higher dipole moment of **S1-Cu** reflects greater charge asymmetry, likely due to the meta-substitution disrupting molecular symmetry compared to the more symmetric para-arrangement in **S2-Cu**. **S2-Cu**, with its higher η and E_{gap}, exhibits lower reactivity, making it well-suited for stable applications. In contrast, the high ω and μD calculated for **S1-Cu** indicate greater electrophilicity and polarity, suggesting potential utility in reactive roles such as catalysis. Polarizability (α), which measures the deformability of the electron cloud in an electric field, is slightly higher in **S2-Cu**. This increase likely stems from enhanced conjugation due to para-substitution, making it more responsive to external electric fields.

The frontier molecular orbital diagrams are presented in **Figure 7**, illustrating the spatial distribution of the highest occupied molecular orbital (HOMO) and the lowest unoccupied molecular orbital (LUMO). In **Figure 7(a)**, the HOMO exhibits π character and is predominantly localized on one side of the salicylaldehyde moiety. In contrast, the corresponding LUMO displays π* character and is distributed across the entire salicylaldehyde unit. Similarly, in

Figure 7(b), the HOMO is localized on one of the salicylaldehyde moieties and retains π character, while its LUMO counterpart also shows π* character with a comparable distribution across the same region. The kind of transitions involved in both compounds are π→π* transition.

DNA binding study

For any given DNA, a major groove or a minor groove separation is expected. To analyze an optically active material such as DNA, amino acids and proteins, circular dichroism (CD) spectroscopy is employed. CD signals are also used to determine conformational changes and mode of interaction between biological molecules and therapeutic agents [35]. The CD can also monitor the conformational transition of DNA. In our study, CT-DNA conformation showed two distinctive bands in the CD spectrum, a positive band at 275 nm (due to base stacking) and a negative band at around 245 nm (due to polynucleotide helicity) which are the characteristic features of DNA in its right-handed B form. The interaction was observed on DNA:metal complex base pair ratio. Circular dichroism spectroscopy (Figure 8) shows the B-DNA structure retained both at low and at higher loading of the copper complexes. It is possible that the complexes are not perturbing the B-DNA conformation as some metal complexes do, but only a minor binding into the groove was observed for both complexes. Circular dichroism spectroscopy indicates that the interaction of complexes **S1-Cu** and **S2-Cu** with DNA is weak, not of an intercalative nature, but may be due mainly to electrostatic and H-bonding type of interactions [36], this corroborates the molecular docking results as revealed in Figure 10. The copper(II) complexes, on the other hand, did not display additional bands which may be attributed to charge-transfer transitions [37].

Molecular docking

Figure 9 shows the structures of synthesized complexes alongside reference drugs docked against CDK7 while Table 2 shows the binding energies of the synthesized copper complexes with human CDK7. Significantly, the binding energies of the complexes were far more than what were obtained for the reference drugs. The 3D image extraction and analysis of docking results obtained using DS studio receptor-complex interaction are shown in Figures 10 (A-D) and 11 (A-D).

It is obvious that synthesized compounds **S2-Cu** and **S1-Cu** complexes far outperformed the three selected standard drugs used as reference. **S2-Cu** complex was the most active of all compounds tested with binding score of -22.60 kcal/mol (Table 2). The presence of binding interactions such as hydrogen bond, alkyl/ π-alkyl, π-sigma, π- π stacked, π-anion/cation, carbon-hydrogen and van der Waals between the lead **S2-Cu** complex (Figure 10B) and the amino acid residues of cyclin-dependent kinase 7 (Figure 10A) such as Tyr27, Lys14, Glu13, Arg30, Thr34, Asp31, Asp79, Lys32 amongst others exhibiting moderate to strong bonding values confirmed the complex as a potential inhibitor. The 3D structure of CDK7 revealing the most active sites (circled in red) (A), **S2-Cu** complex `(B), interacting residues of CDK7 with **S2-Cu** complex (C) and its extended interacting effects within active site of CDK7 (D) is shown in Figure 10A-D.

The solvent accessible surface area provides insights into the structural folding/unfolding dynamics of a protein molecule in the aqueous environment and it is the extent to which atoms on the surface of a protein can form contacts with solvent [38] while hydrophobic/hydrophilic interactions also ensure the protein is stable and biologically active through decrease in surface area, thereby reducing the undesirable interactions with water where necessary. The information obtained could be helpful to analyze if the complex is retained inside the binding pockets of the protein [39]. Compound **S2-Cu** complex inhibitory potential as an anticancer agent was also revealed in its total hydrophobic (Figure 11C) and solvent accessibility (Figure 11D) interactions with the amino acid residues of CDK7 showing its desirability, stability and biologically activity necessary in binding interactions, thus showing the drug-likeness, inhibitory properties and ability of the metal complex to dissolve in the cell fatty layers such as fatty acids, cholesterol, and lipophilic hormones [40] with good solvent accessibility. Some unique features such as charge-to-charge π-anion/cation interaction and strong hydrogen bonding was observed between the oxygen atom of Asp31 and hydrogen atom of Glu13 respectively to the oxygen atoms of **S2-Cu** complex on one side of the complex while an unfavorable interaction Lys14 was observed from the other side (**Figure 12**). To avoid unfavorable interactions, selection of the best geometry/positioning of the complex within the active pockets of the protein was necessary and this was taken care of during mode selection in the course of the docking.

Bioactivity score

To predict the bioactivity of synthesized complexes (alongside the selected reference drugs for comparison purpose) drug-likeness analysis was employed where the SMILES representations of the compounds were submitted to Molinspiration web server (https://www.molinspiration.com/) and the resulting data carefully extracted and examined. The drug likeness/bioactivity scores obtained for G-protein-coupled receptors (GPCR) ligand, ion channel modulator (ICM), kinase inhibitor (KI), nuclear receptor ligand (NRL), protease inhibitor (PI) and enzyme inhibitor EI) are presented in **Figure 13**. For an average bioactive molecule, the bioactivity score when greater than 0.00 is defined as active, - 0.50 to 0.0 is moderately active, and if less than - 0.50 then inactive [41]. **Figure 13** revealed that synthesized **S2-Cu** and **S1-Cu** complexes competes effectively with Epirubicin and Capecitabine while 5-Fluorouracil fell below the bioactivity standards.

Comparison of toxicity prediction of synthesized compounds with reference drugs

The synthesized **S1-Cu** and **S2-Cu** complexes and the selected common references were also subjected to toxicity testing by inputting their SMILES representation (drawn using ChemDraw 14.0 and saved as an.sdf file) into Protox II web server (https://tox-new.charite. de/protox_II/). The web server provided data on hepatoxicity, carcinogenicity, immunotoxicity, mutagenicity, cytotoxicity, amongst others which were then extracted [42, 43]. The results obtained as shown in **Table 3** revealed that the synthesized compounds **S1-Cu** and **S2-Cu** complexes are less toxic when compared with all the reference drugs.

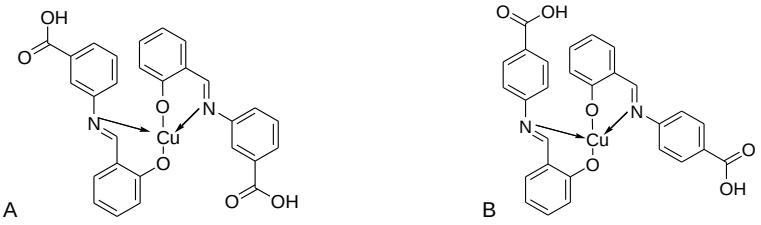

Figure 1: Schiff base copper complexes (A=S1-Cu complex) and (B=S2-Cu complex)

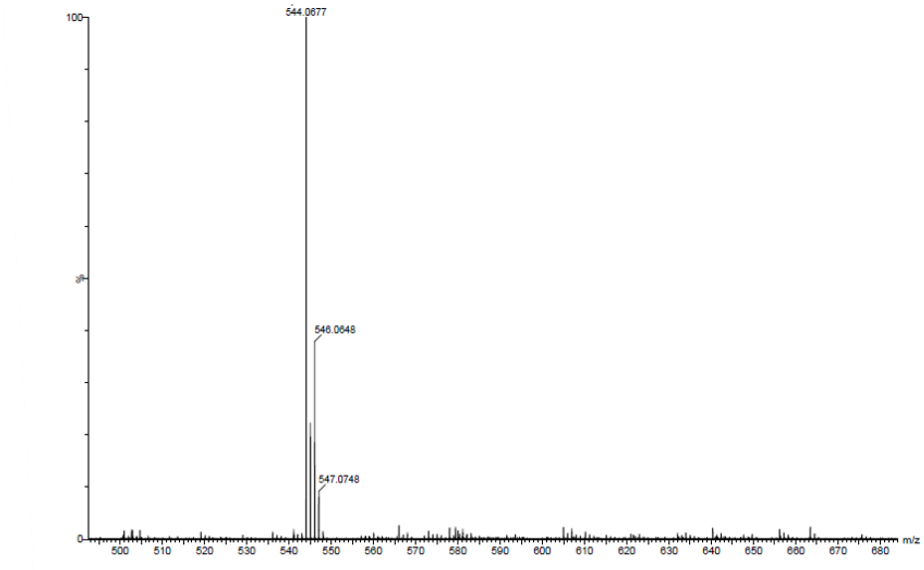

Figure 2. ESI-MS of S1-Cu, ESI-MS: 544.06; m/z: $[M+H]^+$ 544.06

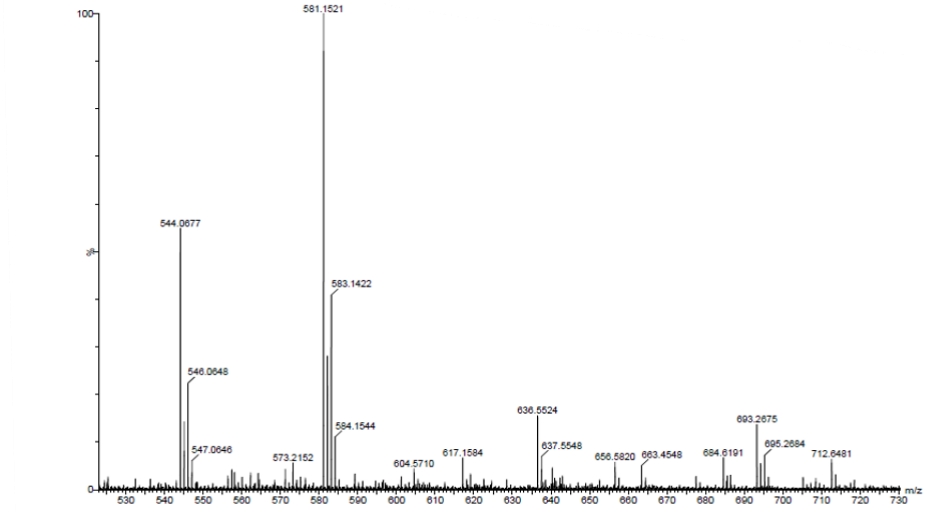

Figure 3. ESI-MS for S2-Cu, ESI-MS: 544.06 ; m/z: $[M+H]^+$ 544.06

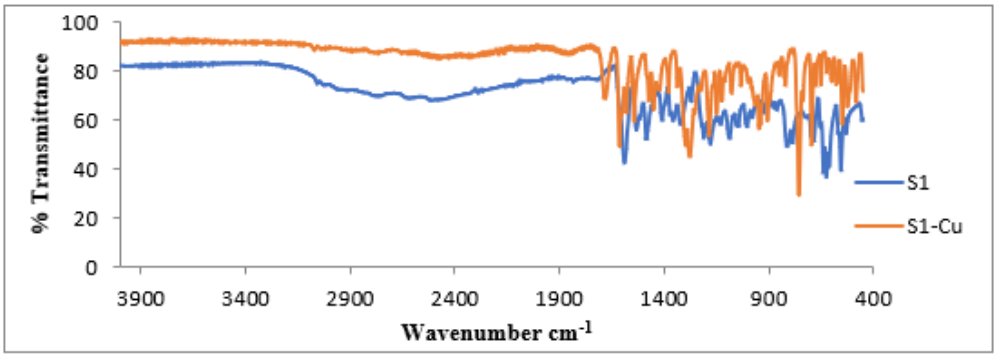

A

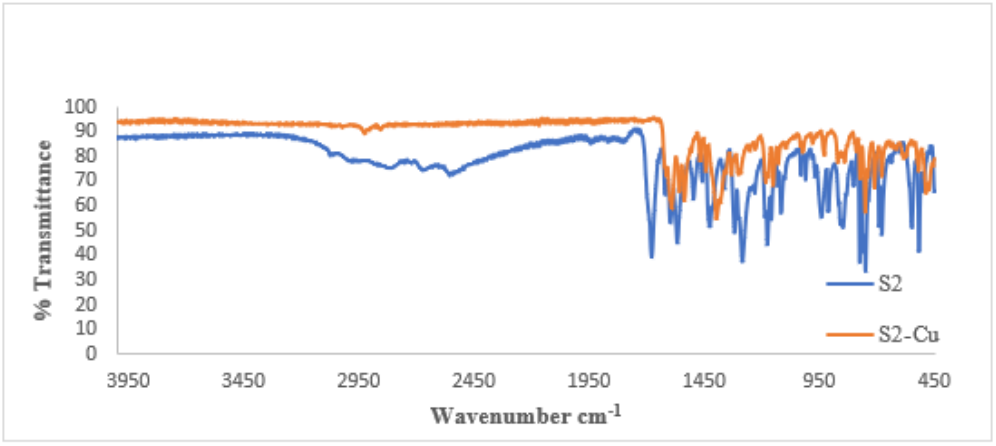

B

Figure 4. FTIR of (A=S1 and S1-Cu) and (B=S2 and S2-Cu)

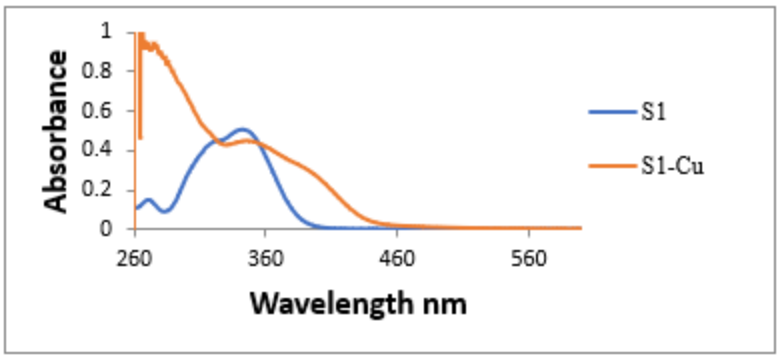

A

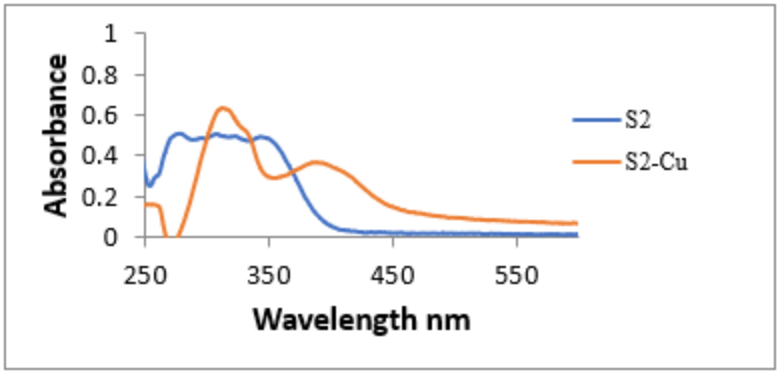

B

Figure 5. UV-vis of (A=S1 and S1-Cu complex**)** and **(**B=S2 and S2-Cu)

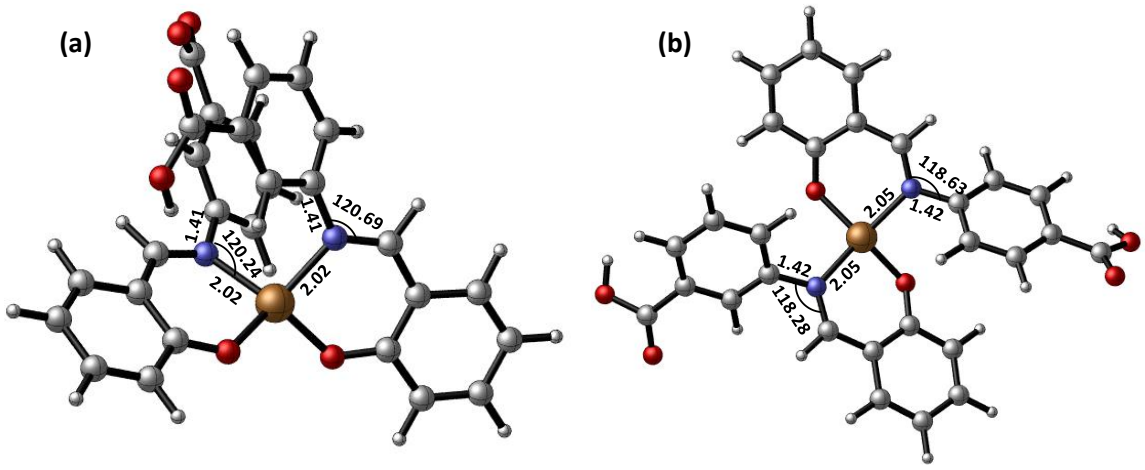

Figure 6. The optimized structures of **(a)** S1-Cu and **(b)** S2-Cu.
The optimization was performed with the M062X method. The bond lengths and angles are presented in angstrom (Å) and degree (˚)

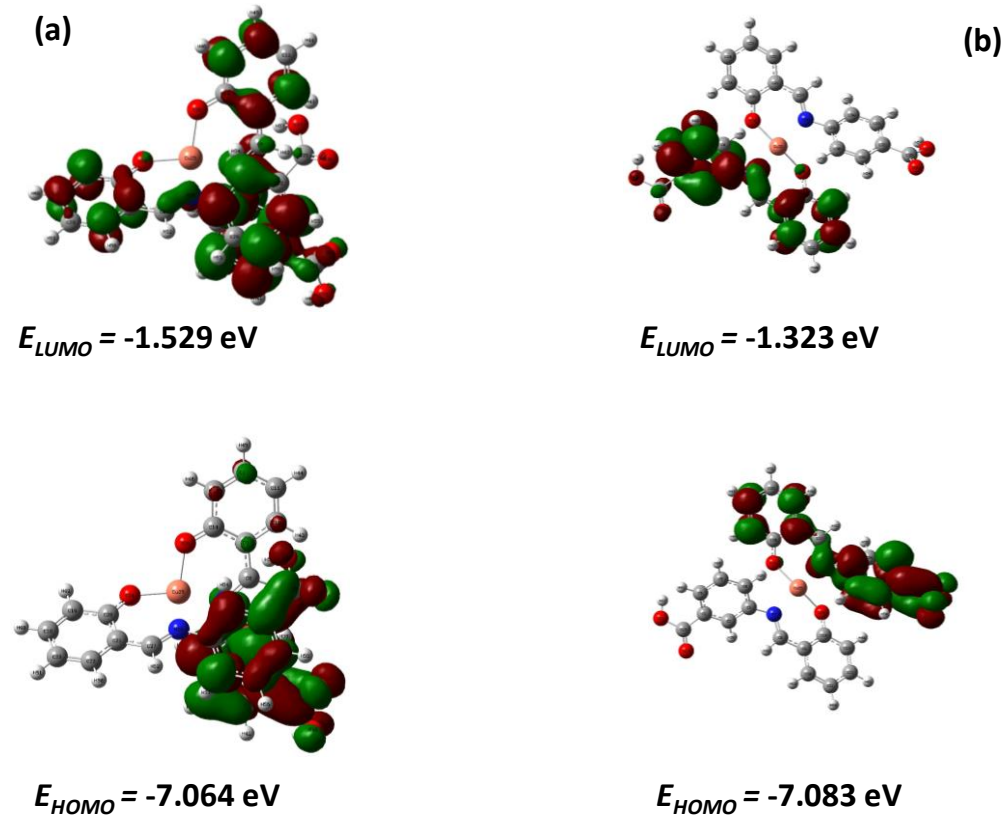

Figure 7. The FMOs of the complexes, calculated using the M062X DFT method. **(a)** S1-Cu and **(b)** S2-Cu

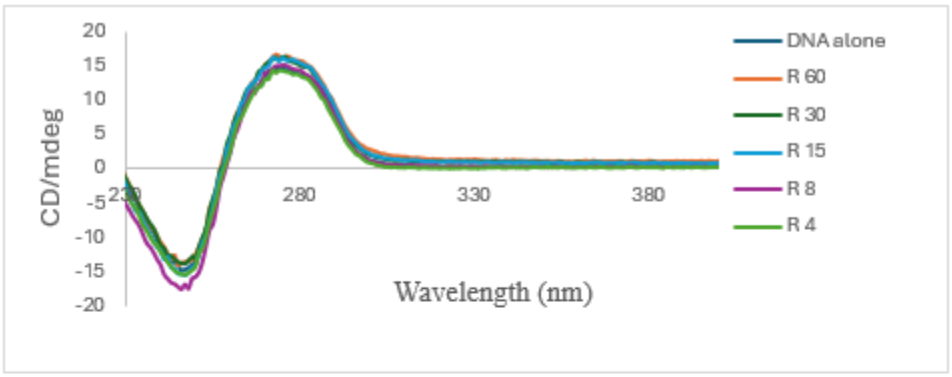

8A

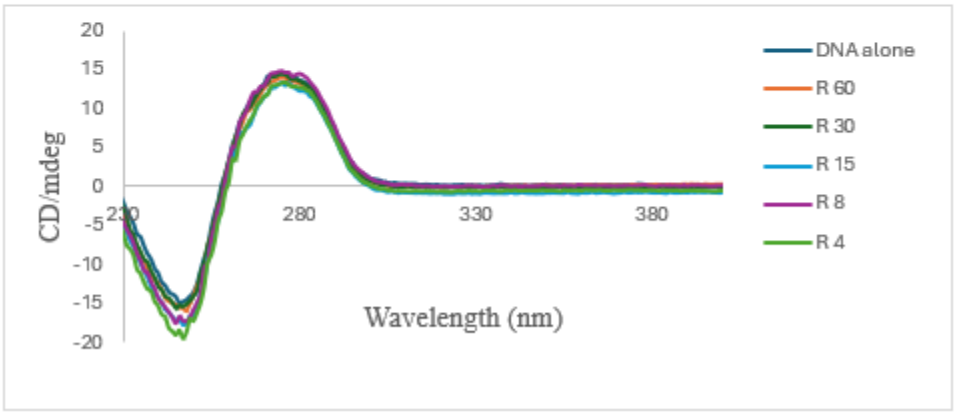

8B

Figure 8. Circular dichroism showing interaction of copper complexes with DNA.
Ct DNA=100 µM; 1% DMSO (A, S1-Cu; 200 µM), (B, S2-Cu; 200 µM)

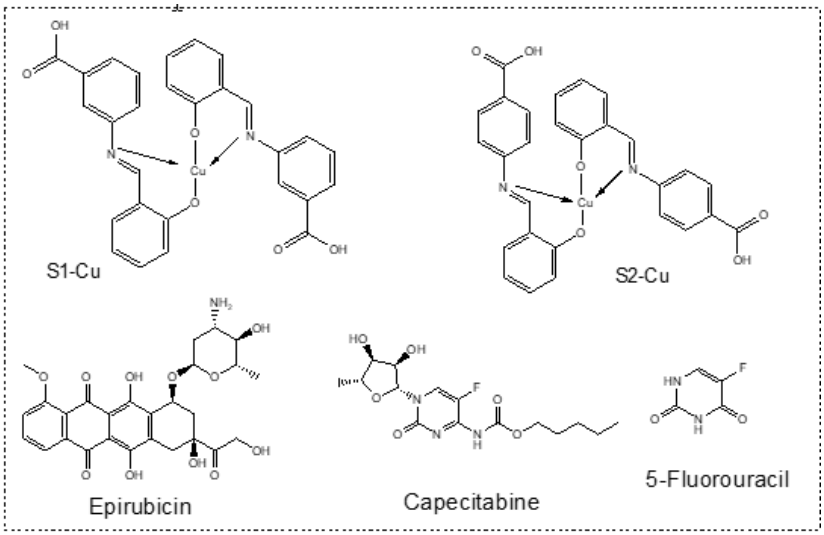

Figure 9. Structures of synthesized complexes and reference drugs used for docking study

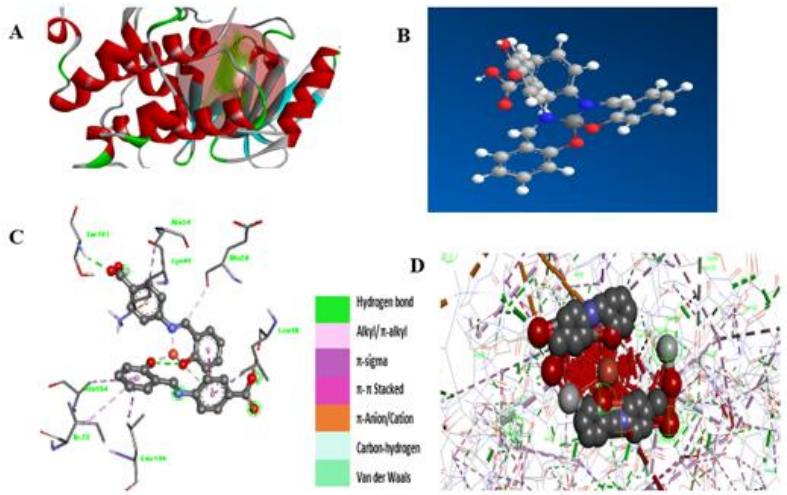

Figure 10. 3D structure of CDK7 revealing the most active sites (circled in red) (A). S2-Cu complex (B). Interacting residues of CDK7 with S2-Cu complex (C). Extended interacting effects of S2-Cu complex within active site of CDK7 (D).

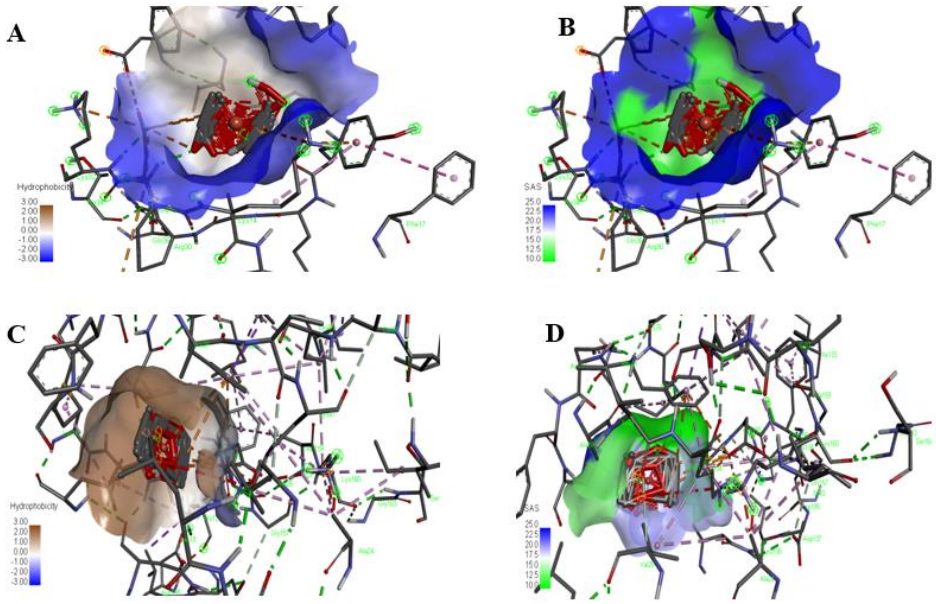

Figure 11. 3D structures of CDK7-S1-Cu complex (A and B) and CDK7-S2-Cu complex (C and D) showing hydrophobic/hydrophilic (A and C) and solvent accessibility surface (B and D) interactions respectively.

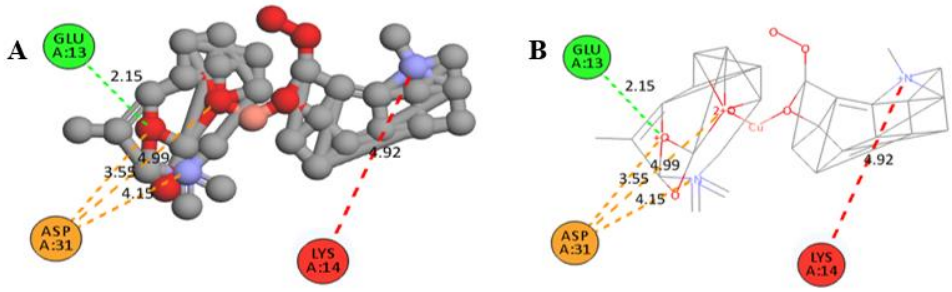

Figure 12. 3D ball and stick (A) and line (B) structures of CDK7-S2-Cu complex interactions, bond distances and key atomic charge-to-charge and hydrogen bond interactions.

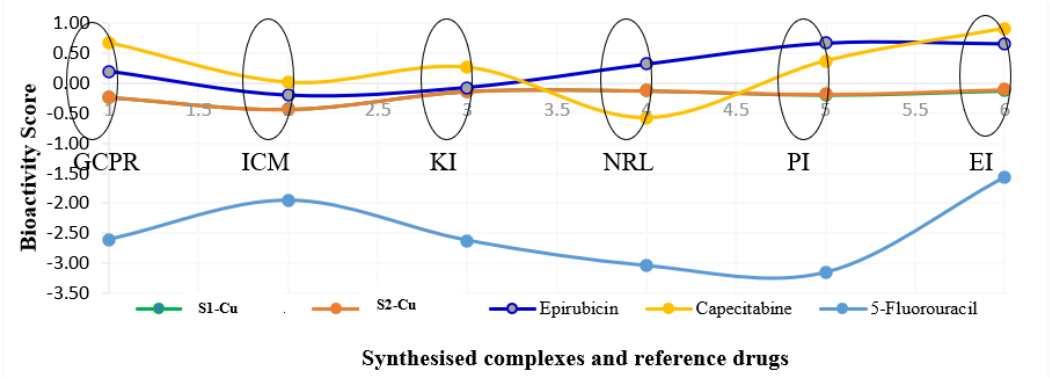

Figure 13. Bioactivity scores of synthesized complexes and three anticancer reference drugs

Table 1. The calculated electronic properties of the metal complexes performed at the M062X DFT method.

Electronic properties	S1-Cu	S2-Cu
E(N) (a.u.)	-1835.4342	-1835.4307
E(N-1) (a.u.)	-1835.1328	-1835.1319
E(N+1) (a.u.)	-1835.5303	-1835.5186
VIP (eV)	8.202	8.130
VEA (eV)	2.615	2.391
η (eV)	5.587	5.738
μ (eV)	-5.409	-5.260
ω (eV)	2.618	2.411
E_{HOMO} (eV)	-7.064	-7.083
E_{LUMO} (eV)	-1.529	-1.323
E_{gap} (eV)	5.535	5.760
α (a.u.)	388.099	389.208
μ_D (Debye)	7.57	5.96

Table 2. Summary of binding energies of copper complexes and anticancer reference drugs
RMSD/UB=root mean square deviation/upper bound; RMSD/LB= root mean square deviation/lower bound

Ligand-metal-protein complex	Binding affinity (kcal/mol)	RMSD/UB	RMSD/LB
1UA2_S2-Cu	-22.60	0	0
1UA2_S1-Cu	-22.00	0	0
1UA2_Epirubicin (ID: 41867)	-10.30	0	0
1UA2_Capecitabine (60953)	-7.80	0	0
1UA2_5-Fluorouracil (3385)	-5.20	0	0

Table 3. Toxicity prediction and probability of synthesized complexes and common anticancer standard drugs using Protox II webserver

Toxicity Targets	S1-Cu	S2-Cu	Epirubicin	Capecitabine	5-Fluorouracil
Hepatotoxicity	Active (0.55)	Active (0.55)	Inactive (0.86)	Active (0.56)	Inactive (0.78)
Neurotoxicity	Inactive (0.74)	Inactive (0.74)	Active (0.74)	Active (0.91)	Active (0.90)
Nephrotoxicity	Active (0.63)	Active (0.63)	Active (0.80)	Active (0.86)	Inactive (0.51)
Respiratory toxicity	Active (0.50)	Active (0.50)	Active (0.91)	Active (0.92)	Active (0.72)
Cardiotoxicity	Inactive (0.66)	Inactive (0.66)	Active (0.64)	Inactive (0.76)	Inactive (0.89)
Carcinogenicity	Inactive (0.63)	Inactive (0.63)	Inactive (0.90)	Inactive (0.61)	Active (0.85)
Immunotoxicity	Inactive (0.98)	Inactive (0.99)	Active (0.99)	Active (0.97)	Inactive (0.99)
Mutagenicity	Inactive (0.54)	Inactive (0.54)	Active (0.98)	Inactive (0.72)	Inactive (0.88)
Cytotoxicity	Inactive (0.68)	Inactive (0.68)	Active (0.94)	Inactive (0.75)	Inactive (0.93)
BBB-barrier	Inactive (0.56)	Inactive (0.56)	Inactive (1.0)	Inactive (0.52)	Active (0.89)

Conclusion

As a conclusion, the present study shows the prospects of Schiff base copper complexes containing aminobenzoic acid moiety **S1-Cu** and **S2-Cu** as potential cell inhibitor of cyclin-dependent kinase 7. The complexes binding positions were deduced from in-silico study and serves as a lead towards exploring other complexes of different moiety. **S2-Cu** complex was the most active of the compounds tested. A deeper understanding of CDK7 biology and selection of specific cancer types for personalized therapeutics continues. Further research and in-depth study will reveal the true value of this therapeutic strategy.

Abbreviations

CD: circular dichroism
CDK 7: cyclin-dependent kinase 7
CT-DNA: calf thymus-deoxyribonucleic acid
DNA: Deoxyribonucleic acid
ESI-MS: Electrospray ionization mass spectrometry
FTIR: Fourier Transform Infrared Spectroscopy,
RNA: Ribonucleic acid
SCF: Self-consistent field
TD-DFT: time-dependent density functional theory
VEA: vertical electron affinity
VIP: vertical ionization potential

Authors' Contribution

FNE, OSA and IAU carried out the study; TMF and OBF supervised the study; All authors read and approved the final version of the manuscript.

Acknowledgments

The authors are grateful to the Department of Chemistry, University of Birmingham where the characterization analysis was carried out.

Conflict of interest

The authors declare no conflict of interest

Article history:
Received: 19 May 2025
Received in revised form: 11 June 2025
Accepted: 11 June 2025
Available online: 12 June 2025

References

1. Belew MD, Chen J, Cheng Z. 2025. Emerging roles of cyclin-dependent kinase 7 in health and diseases. *Trends Mol Med*. 31(2):138-151
2. Feaver WJ, Svejstrup JQ, Henry NL, Kornberg RD. 1994. Relationship of CDK-activating kinase and RNA polymerase II CTD kinase TFIIH/TFIIK. *Cell*. 79(6):1103-1109.
3. Lu H, Zawel L, Fisher L, Egly JM, Reinberg D. 1992. Human general transcription factor IIH phosphorylates the C-terminal domain of RNA polymerase II. *Nature*. 358(6388):641-645.
4. Shilatifard A, Conaway RC, Conaway JW. 2003. The RNA polymerase II elongation complex. *Annu Rev Biochem*. 72(1):693-715.
5. Sava GP, Fan H, Coombes RC, Buluwela L, Ali S. 2020. CDK7 inhibitors as anticancer drugs. *Cancer Metastasis Rev*. 39, 805-823.
6. Pellarin I, Dall'Acqua A, Favero A, Segatto I, Rossi V, Crestan N, Karimbayli J, Belletti B, Baldassarre G. 2025. Cyclin-dependent protein kinases and cell cycle regulation in biology and disease. *Signal Transduct Target Ther*. 10(1):11.
7. Espinosa JM. 2019. Transcriptional CDKs in the spotlight. *Transcription*. 10(2):45-46.
8. Patel H, Periyasamy M, Sava GP, Bondke A, Slafer BW, Kroll SHB, Barbazanges M, Starkey R, Ottaviani S, Harrod A, Aboagye EO, Buluwela L, Fuchter MJ, Barrett AGM, Coombes RC, Ali S. 2018. ICEC0942, an Orally Bioavailable Selective Inhibitor of CDK7 for Cancer Treatment. *Mol Cancer Ther*. 17(6):1156-1166
9. Hu S, Marineau JJ, Rajagopal N, Hamman KB, Choi YJ, Schmidt DR, Ke N, Johannessen L, Bradley MJ, Orlando DA, Alnemy SR, Ren Y, Ciblat S, Winter DK, Kabro A, Sprott KT, Hodgson JG, Fritz CC, Carulli JP, di Tomaso E, Olson ER. 2019. Discovery and Characterization of SY-1365, a Selective, Covalent Inhibitor of CDK7. *Cancer Res.* 79(13):3479-3491.
10. Bashir B, Sharma M, Juric D, Papadopoulos KP, Hamilton EP, Richardson DL, Shapiro G, Sahai V, Mettu NB, Wainberg ZA, Alese OB, Dragovich T, Hodgson G, Henry S, Hall T, Paul S, Roth DA, Kelly M, Malak TA, Klimek V. 2023. Phase 1/1b study of SY-5609, a selective and potent CDK7 inhibitor, in advanced solid tumors and in 2L/3L pancreatic ductal adenocarcinoma (PDAC) in combination with gemcitabine +/- nab-paclitaxel. *J Clin Oncol*. 41, 3080-3080.
11. Chipumuro E, Marco E, Christensen CL, Kwiatkowski N, Zhang T, Hatheway CM, Abraham BJ, Sharma B, Yeung C, Altabef A, Perez-Atayde A, Wong KK, Yuan GC, Gray NS, Young RA, George RE. 2014. CDK7 inhibition suppresses super-enhancer-linked oncogenic transcription in MYCN-driven cancer. *Cell*. 159(5):1126-1139.
12. Ali S, Heathcote DA, Kroll SH, Jogalekar AS, Scheiper B, Patel H, Brackow J, Siwicka A, Fuchter MJ, Periyasamy M, Tolhurst RS, Kanneganti SK, Snyder JP, Liotta DC, Aboagye EO, Barrett AG, Coombes RC. 2009. The development of a selective cyclin-dependent kinase inhibitor that shows antitumor activity. *Cancer Res*. 69(15):6208-15.
13. Lolli G, Lowe ED, Brown NR, Johnson LN. 2004. The crystal structure of human CDK7 and its protein recognition properties. *Structure*. 12(11):2067-2079.
14. Bartkova J, Zemanova M, Bartek J. 1996. Expression of CDK7/CAK in normal and tumor cells of diverse histogenesis, cell-cycle position and differentiation. *Int J Cancer*. 66(6):732-7
15. Carlson BA, Dubay MM, Sausville EA, Brizuela L, Worland PJ. 1996. Flavopiridol induces G1 arrest with inhibition of cyclin-dependent kinase (CDK) 2 and CDK4 in human breast carcinoma cells. *Cancer Res*. 56(13):2973-8
16. Chen R, Keating MJ, Gandhi V, Plunkett W. 2005. Transcription inhibition by flavopiridol: mechanism of chronic lymphocytic leukemia cell death. *Blood*. 106(7):2513-9
17. Mughal MJ, Bhadresha K, Kwok HF. 2023. CDK inhibitors from past to present: A new wave of cancer therapy. *Semin Cancer Biol*. 88, 106-122
18. Ashraf T, Ali B, Qayyum H, Haroone MS, Shabbir G. 2023. Pharmacological aspects of Schiff base metal complexes: A critical review. *Inorg Chem Commun*. 150, 110449.
19. Thakur S, Jaryal A, Bhalla A. 2024. Recent advances in biological and medicinal profile of Schiff bases and their metal complexes: An updated version (2018-2023). *Results Chem.* 7, 101350
20. Yadav A, Poonia K. 2024. Recent advances on the DNA interaction properties of Schiff bases and their metal complexes. *Appl Organomet Chem*. 38(6):e7496
21. El-Afify ME, Elsayed SA, Shalaby TI, Toson EA, El-Hendawy AM. 2021. Synthesis, characterization, DNA binding/cleavage, cytotoxic, apoptotic, and antibacterial activities of V(IV), Mo(VI), and Ru(II) complexes containing a bioactive ONS-donor chelating agent. *Appl Organomet Chem*. 35(2):e6082.
22. Mansi B, Charu K, Pankaj J, Manisha T, Sangeeta Y, Shilpa K, Leena. 2023. The Recent Report on Schiff Bases and their Complexes as DNA Binders. *Curr Org Chem*. 27(20):1799-1813(15)
23. Ejiah FN, Fasina TM, Familoni OB, Ogunsola, FT. 2013. Substituent effect on spectral and antimicrobial activity of Schiff bases derived from aminobenzoic acids. *Adv Biol Chem*. **3**, 475-479
24. Zhao Y, Truhlar DG. 2006. A Comparative DFT Study of van der Waals Complexes: Rare-Gas Dimers, Alkaline-Earth Dimers, Zinc Dimer, and Zinc-Rare-Gas Dimers. *J Phys Chem. A*. 110, 5121-5129
25. Rassolov VA, Ratner MA, Pople JA, Redfern PC, Curtiss LA. 2001. 6-31G* basis set for third-row atoms. *J Comput Chem*. 22(9):976-984.
26. Dooley R, Milfeld K, Guiang C, Pamidighantam S, Allen G. 2006. From proposal to production: Lessons learned developing the computational chemistry Grid cyberinfrastructure. *J Grid Comput.* 4(2):195-208.
27. Pamidighantam S, Nakandala S, Abeysinghe E, Wimalasena C, Yodage SR, Marru S, Pierce M. 2016. Community Science Exemplars in SEAGrid Science Gateway: Apache Airavata Based Implementation of Advanced Infrastructure. *Procedia Computer Science*. 80(1):1927–1939.
28. Shen N, Fan Y, Pamidighantam S. 2014. E-science infrastructures for molecular modeling and parametrization. *J Comput Sci*. 5(4):576-589.
29. Trott O, Olson AJ. 2010. AutoDock Vina: Improving the speed and accuracy of docking with a new scoring function, efficient optimization, and multithreading. *J Comput Chem*. 31:455.
30. Copeland RA. 2013. Evaluation of Enzyme Inhibitors in Drug Discovery: A Guide for Medicinal Chemists and Pharmacologists. United States: *John Wiley & Sons*. 576pp
31. Ramesh G, Daravath S, Babu KJ, Dharavath R, Ranjan A, Ayodhya D, Shivaraj. 2025. Design, Synthesis, Structural Investigation and Photo Induced Biological Investigations of Co(II), Ni(II) and Cu(II) Complexes Derived from N,O Donor Schiff Bases. *J Fluoresc*. 35(4):2087-2108.
32. Nemati BB, Sousaraei A, Moghadam M. 2024. Unveiling the key role of metal coordination mode and ligand's side groups on the performance of deep-red light-emitting electrochemical cell. *Sci Rep*. 14(1):16070.
33. Richter J, Liebing P, Edelmann FT. 2018. Early transition metal and lanthanide metallocenes bearing dihydroazulenide ligands. *Inorg Chim Acta*. 475, 18-27.
34. Ramesh P, Caroline ML, Muthu S, Narayana B, Raja M, Aayisha S. 2020. Spectroscopic and DFT studies, structural determination, chemical properties and molecular docking of 1-(3-

bromo-2-thienyl)-3-[4-(dimethylamino)-phenyl] prop-2-en-1-one. *J Mol Struct.* 1200, 127123.
35. Pakravan P, Masoudian S. 2015. Study on the Interaction between Isatin-β-Thiosemicarbazone and Calf Thymus DNA by Spectroscopic Techniques. *Iran J Pharm Res.* 14(1):111-23.
36. Arbuse A, Font M, Martínez MA, Fontrodona X, Prieto MJ, Moreno V, Sala X, Llobet A. 2009. DNA-Cleavage Induced by New Macrocyclic Schiff base Dinuclear Cu(I) Complexes Containing Pyridyl Pendant Arms. *Inorg Chem*. 48 (23):11098-11107.
37. Downing RS, and Urbach FL. 1969. Circular dichroism of square-planar, tetradentate Schiff base chelates of copper(II). *J Am Chem Soc*. 91(22):5977-5983.
38. Savojardo C, Manfredi M, Martelli PL, Casadio R. 2021. Solvent accessibility of residues undergoing pathogenic variations in humans: from protein structures to protein sequences. *Front Mol Biosci*. 7, 626363.
39. Ma FH, Li C, Liu Y, Shi L. 2020. Mimicking molecular chaperones to regulate protein folding. *Adv Mater*. 32(3):1805945.
40. McEwan IJ. 2009. Nuclear receptors: One big family. *Methods Mol Biol*. 505:3-8.
41. Khan H, Khan Z, Amin S, Mabkhot YN, Mubarak MS, Hadda TB, Maione F. 2017. Plant bioactive molecules bearing glycosides as lead compounds for the treatment of fungal infection: A review. *Biomed Pharmacother.* 93: 498-509.
42. Banerjee P, Eckert AO, Schrey AK, Preissner R. 2018. ProTox-II: a webserver for the prediction of toxicity of chemicals. *Nucleic Acids Res.* 46(1):257-263.
43. Drwal MN, Banerjee P, Dunkel M, Wettig MR, Preissner R. 2014. ProTox: a web server for the in-silico prediction of rodent oral toxicity. *Nucleic Acids Res.* 42(1):53-58.